Beyond simple dilution: superior conductivities from co-solvation of an acetonitrile/LiTFSI concentrated solution with acetone

Murillo L. Martins[§*], Robert L. Sacci[†*], Xiaobo Lin[‡], Ray Matsumoto[‡], Ivan Popov[†], Jinlei Cui[¥], Takeshi Kobayashi[¥], Madhusudan Tyagi[ǁ], Wei Guo[†], Sheng Dai[†], Marek Pruski[¥], Peter T. Cummings[‡], Alexei P. Sokolov[†,!], Eugene Mamontov[§*].

§Neutron Scattering Division, Oak Ridge National Laboratory, P.O. Box 2008 MS6455, Oak Ridge, Tennessee 37831, United States

†Chemical Sciences Division, Oak Ridge National Laboratory, Oak Ridge, Tennessee 37831, United States

‡Department of Chemical and Biomolecular Engineering, Vanderbilt University, Nashville, Tennessee 37235, United States

¥ U.S. DOE Ames Laboratory, Iowa State University, Ames, Iowa 50011, United States

ǁ NIST Center for Neutron Research, National Institute of Standards and Technology, Gaithersburg, Maryland 20899, United States and Department of Materials Science and Engineering, University of Maryland, College Park, MD 20742, United States

!Department of Chemistry, University of Tennessee, Knoxville, Tennessee 37996, United States

ABSTRACT: Concentrated solutions of Li-salts in acetonitrile are promising alternative electrolytes for the next generation of Li batteries as they may exhibit superior electrochemical properties. However, the reduced mobility of the chemical species is a barrier yet to be overcome and, for this, we explore the utilization of acetone as a co-solvent. Although acetone is a polar compound, we find that its addition to the LiTFSI/acetonitrile solution does not follow the trends expected for a simple dilution process. At a low concentration, acetone subtly shifts acetonitrile from the first to extended solvation sheaths of the ions. Still, most of the original structure of the solution is preserved and mobile high-concentration clusters are formed in the solution. At higher concentrations, the co-solvation promotes cation-anion interactions but with a different nature from those in the original solution and still allows for a further increase in conductivity. Additionally, the non-coordinating fraction of acetonitrile acquires features resembling the pure solvent, which is a possible additional facilitating factor for ionic diffusion.

Introduction

Although Li-batteries are vastly used to power electronic devices[1–3], further developments are needed to meet the demands of present and future applications. For example, while the current state-of-the-art electrolytes based on $LiPF_6$ solutions in ethylene carbonate provide high voltages and efficiently prevent the cathode's degradation, they are flammable, non-environment-friendly, and unstable in the presence of water traces[4]. Hence, different options have been explored as next-generation electrolytes, including aqueous solutions and ionic liquids. Nevertheless, water's narrow electrochemical voltage and ionic liquids' high viscosity restrict their applications[5,6]. Within this context, highly concentrated solutions of Li-salts in organic solvents are emerging alternatives, especially when they reach salt/solvent weight and/or volume ratios > 1[7]. In particular, concentrated solutions of Lithium-bis(trifluoromethanesulfonyl)imide (LiTFSI) in acetonitrile have been widely investigated[8–10] and with this combination, Li^+ is coordinated by up to six solvent molecules that are, therefore, scarce in the free form. As for $TFSI^-$, it may directly coordinate the cations, form solvent-separated ion pairs, be found as uncoordinated species or individual solvent-anion complexes[11].

From a positive perspective, the abundant ion-ion interactions in concentrated solutions allow for achieving unique electrochemical properties[7,12,13]. However, their commercial utilization as electrolytes is still limited by characteristics associated with the high salt concentrations, namely: high costs, high viscosity, and the tendency of salt precipitation at low temperatures[4]. The poor ionic conductivities are also a limiting characteristic[14] and in such a saturated environment, the ionic transport cannot be solely explained by vehicular mechanism. Therefore, different mechanisms have been suggested based on, for example, ligand exchange [15] and the formation of bulk-like diffusive channels[16] or percolating networks[17,18].

In this work, we explore the concept of co-solvation to improve the conductivity of a highly concentrated LiTFSI/acetonitrile solution while preserving the abundance of ion-ion interactions. Once a stable and soluble co-solvent is added to this system, the viscosity decreases, increasing the overall diffusivities. Ideally, a low polar co-solvent should act as an inert component, and high-concentration clusters would move through the solution[4,19]. With this presumption, we recently explored the addition of chloroform to an acetonitrile/LiTFSI solution[20] and did observe an improvement in the overall diffusivities. Nevertheless, the co-solvent led to the exacerbated formation of cation-anion correlations and, consequently, ionic aggregates, which rapidly suppress the room temperature conductivity, as also reported with hydrofluoroether being added to triglyme/LiTFSI concentrated solutions[21].

Here, we use a co-solvent, acetone, whose dipole moment and dielectric constant at room temperature are comparable but still lower than of acetonitrile – $\text{acetonitrile}_{\text{dipole moment}} = 3.92$ *vs* $\text{acetone}_{\text{dipole moment}} = 2.69$; $\text{acetonitrile}_{\text{dielectric constant}} = 37.5$ *vs* $\text{acetone}_{\text{dielectric constant}} = 20.7$[22]. Then, acetone was added to an acetonitrile/LiTFSI = 3:1 (molar ratio) solution and, as somewhat expected, behaves as an active co-solvent gradually shifting acetonitrile to extended solvation shells. Nevertheless, the consequences of this mechanism are concentration-dependent, and the solutions can be tailored to achieve higher conductivities than those obtained with a simple increase in acetonitrile content. At a low concentration, acetone does not drastically change the original solvation structures and high-concentration clusters are formed in the solution without increasing the content of free acetonitrile. At higher concentrations, acetone reduces the participation of acetonitrile and $TFSI^-$ in the cations' first solvation sheath but cation-anion interactions with a different nature are still promoted. Additionally, the non-coordinating acetonitrile molecules exhibit vibrational features resembling the pure solvent, as detected by infrared spectroscopy, which possibly facilitates ionic diffusion.

Materials and Methods

Materials and Samples preparation

Protiated acetonitrile (*p*-acetonitrile), deuterated acetonitrile (*d*-acetonitrile), protiated acetone (*p*-acetone), deuterated acetone (*d*-acetone), and LiTFSI were purchased from Sigma-Aldrich. All solvents were stored over freshly activated 4A molecular sieves for at least 24 h before use and LiTFSI was dried at 100 °C under vacuum for at least 3 days.

The solutions were prepared in an Ar glovebox by dissolving LiTFSI in either *p*-acetonitrile or d-acetonitrile, depending on the experimental requirements, in an acetonitrile/ LiTFSI = 3:1 molar ratio. Sequentially, either *p*-acetone or *d*-acetone was added to the resulting solutions in three molar ratios: acetone/ acetonitrile/ LiTFSI = 1:3:1, 3:3:1, and 9:3:1 leading to solutions with 5.5, 3.4, and 1.5 $mol.kg^{-1}$ (mols of salt per kg of solvents). For some of the experiments, solutions without the addition of acetone were prepared with the molar ratios of acetone/ acetonitrile/ LiTFSI = 0:3:1 (8.1 $mol.kg^{-1}$) and 0:7.3:1 (3.4 $mol.kg^{-1}$, which is comparable with that of the acetone-containing sample with the composition 3:3:1).

Conductivity experiments

Conductivity measurements were performed on an Alpha-A analyzer from Novocontrol in the frequency range of 10^{-1} Hz to 10^{6} Hz between 190 K and 340 K. The sample with the composition acetone/ acetonitrile/ LiTFSI = 9:3:1 could not be measured up to 340K due to the high vapor pressure of acetone. A cell with a cap as a bottom electrode, fixed electrode distance of 0.4 mm, and diameter of 10.2 mm was used and the samples were placed between the electrodes and measured with a voltage amplitude of 0.1 V. A Quattro temperature controller (Novocontrol) was used for different temperature measurements and the samples were stabilized for 20 minutes at each temperature to an accuracy within ± 0.2 K.

Pulsed-field gradient nuclear magnetic resonance (PFG-NMR)

PFG-NMR experiments were performed on a Bruker Avance Neo spectrometer operated at 9.4 T. The self-diffusion coefficients of acetonitrile and acetone were evaluated by assessing the signals from ^{1}H, while for Li^+ and $TFSI^-$ the signals from ^{7}Li and ^{19}F were evaluated. For the study of the solvents, the solutions were prepared with *p*-acetonitrile and *d*-acetone to evaluate the dynamics from acetonitrile and with *d*-acetonitrile and *p*-acetone to investigate the behavior of acetone. The solutions were measured at 240 K, 260 K, 280 K, and 300 K and the stimulated echo intensities were measured as a function of the gradient strength, with the optimum gradient pulse widths found in the range of 1.2–6.0 ms and the diffusion delays of 20–120 ms. Further experimental details are described elsewhere[23].

Molecular dynamic (MD) simulations

Details of the MD simulations are presented in the Supplementary Information (SI), Section S1. The simulations were initialized with mBuild[24,25] (by using PACKMOL[26]) and parameterized with foyer and GAFF-foyer software packages[27,28]. Both software packages fall under the Molecular Simulation and Design Framework (MoSDeF)[29,30] suite of tools. The whole simulation workflow was managed through the signac Framework[31–33]. In the course of the simulations, partial charges were assigned with RESP through the use of the R.E.D. Server and Gaussian 09[34], following concepts presented in refs.[35–37]. Once initialized and parametrized, the simulations were performed with GROMACS 2020[38] and the analyses of self-diffusivities and radial distribution functions were made with MDTraj[39,40].

Infrared spectroscopy (IR)

IR measurements were performed at room temperature with an Agilent Cary 680 spectrometer equipped with a diamond attenuated total reflection accessory (GoldenGate, Specac) at a resolution of 2 cm^{-1}.

Quasielastic neutron scattering (QENS) measurement and analysis

For the QENS experiments, the samples were loaded into flat aluminum plates and sealed with indium wires in an Ar-filled glovebox. Benefiting from the discrepant neutron incoherent cross-sections of ^{1}H and ^{2}D [41], solutions prepared with *p*-acetonitrile and *d*-acetone were used to investigate the dynamics from acetonitrile while samples with *d*-acetonitrile and *p*-acetone were used to study acetone. QENS measurements were performed at the HFBS spectrometer[42] at the National Institute for Standards and Technology (NIST) Center for Neutron Research (NCNR). With this instrument, temperature-dependent elastic scattering intensity scans were performed between 10 K and 300 K with an instrumental resolution of 0.8 μeV, and mean square displacements (MSD) were obtained as described in the SI (Section S1)[43]. QENS experiments were also performed at the backscattering spectrometer BASIS[44] at the Spallation Neutron Source, Oak Ridge National Laboratory, USA. At this instrument, QENS spectra were collected at 300 K with an instrumental resolution of 3.7 μeV, a vanadium standard was used as the instrumental resolution, and data from an empty sample holder was used for background subtraction. The data analyses were performed using the fitting package qClimax[45] and, following the concepts described in the SI (Section S1), self-diffusion coefficients of acetonitrile and acetone were obtained. At BASIS, we have also investigated the behavior of the solutions under confinement in mesoporous carbon, as described in detail in the SI (Section S3).

Results and discussions

Hereafter, the solutions are referred to considering their acetone/ acetonitrile/ LiTFSI molar ratios (0:3:1, 0:7.3:1, 1:3:1, 3:3:1, and 9:3:1). With these compositions, the acetone-free composition 0:3:1 is our starting point and represents a highly concentrated system with the salt/solvent weight and molar ratios > 1. With 1:3:1, we obtain a still highly concentrated co-solvated system with a salt/solvent volume ratio ~1 and weight ratio > 1. Then, the composition 3:3:1 allows for observing the competitive ionic solvation by the solvents, and 9:3:1 is a limiting case with an excessive addition of acetone. Finally, the composition 0:7.3:1 is an acetone-free solution with the same ionic concentration (in mols of salt per kg of solvent) as the composition 3:3:1. For the NMR-PFG and QENS analyses, protiated and deuterated solvents were combined in the formulation of the solutions, and these are indicated by the indexes *p*- and *d*-, respectively.

Temperature-dependent conductivity measurements are presented in Fig. 1, and the inset shows the conductivities at 298K of the above-cited acetone-containing solutions and solutions with the same ionic concentrations but with acetonitrile as the only solvent (extracted from refs. [46] and [18]). In the acetone-containing compositions 1:3:1 and 3:3:1, the room-temperature conductivities are ~ 40% higher than in the correspondent acetone-free samples but no benefits are observed with 9:3:1 (1.5 $mol.kg^{-1}$). Accordingly, Borodin et al.[18] reported no differences in the conductivities of acetonitrile/ LiTFSI solutions with concentrations ranging from 1 to 2 $mol.kg^{-1}$ at temperatures above 273K indicating that the balance between the factors contributing and those damping the conductivities is subtle at this concentration range. These factors are further discussed in the manuscript.

The diffusivities (*D*) of acetonitrile, acetone, and the ions were determined via PFG-NMR, Fig. 2a and 2b. With the co-solvation, the percolation networks found in highly concentrated solutions are no longer

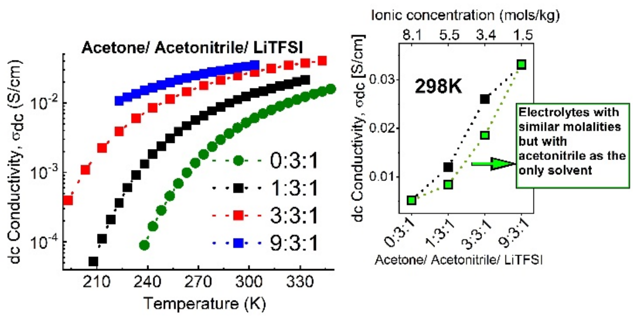

Fig. 1. Temperature-dependent conductivity measurements of solutions with different acetone/ acetonitrile/ LiTFSI molar ratios. The conductivities increase as the ionic concentrations evolve from 8.1 mol.kg^{-1} (0:3:1 in green circles), to 5.5 (1:3:1 in black squares), 3.4 (3:3:1 in red squares), and 1.5 mol.kg^{-1} (9:3:1 in blue squares). The sample with the composition 9:3:1 was not measured up to the highest temperature due to the high vapor pressure of acetone, and the errors in the experiments are smaller than the size of the symbols. In the inset, a comparison is presented between the conductivities at 298K of solutions with the same ionic concentrations with and without acetone (as estimated from refs. [46] and [18]).

expected to be found in the electrolytes or are limited to very small distances. Hence, one can assume that vehicle-type mechanisms dominate the transport properties in the co-solvated solutions. As such, the overall mobility within the solutions, that is the diffusion coefficients of all the chemical species, increases with the addition of acetone following the expected reduction in the viscosities. Still, as discussed further in the manuscript, the solvation structures within the electrolytes can be rather complex in comparison with simply diluted systems.

In all compositions, $D_{acetonitrile} > D_{acetone}$, which may reflect the higher molecular weight of the co-solvent but also suggests that acetone is more often involved in the ions' coordination. As shown in Fig.2a (inset), this difference drops in the composition 9:3:1 indicating an increase in the content of free acetone. In the composition 1:3:1, $D_{Li^+} \approx D_{TFSI^-}$ (Fig. 2b) and with 3:3:1, from 280K to 300K, TFSI$^-$ is more accelerated than any other component in the solution. Consequently, TFSI$^-$ becomes faster than Li$^+$ and this behavior remains in the composition 9:3:1 regardless of the temperature. The evolution of D_{Li^+}/D_{TFSI^-} is highlighted in Fig. 2b (inset). Considering the small ionic radius of Li$^+$ as compared with TFSI$^-$, these results indicate the progressive formation of large solvation structures around the cations.

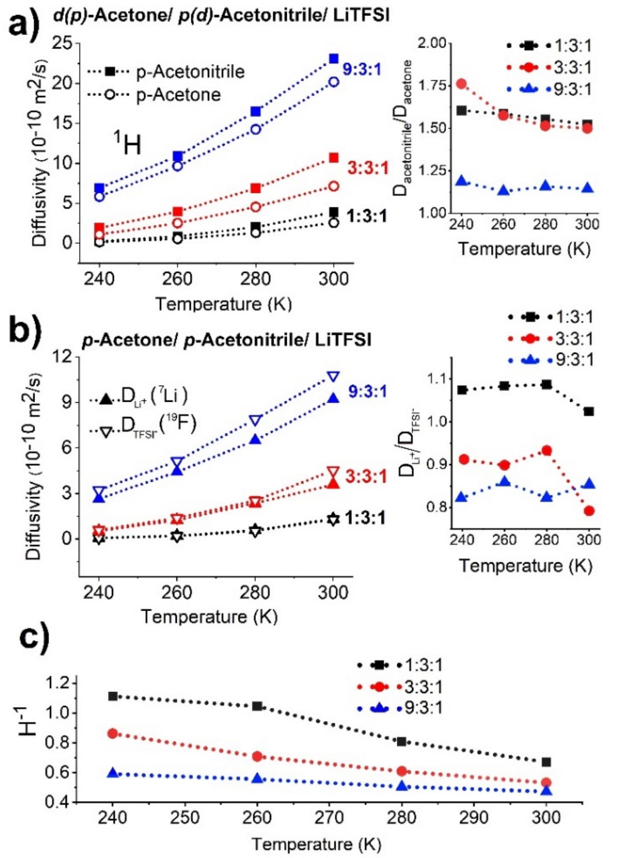

Fig. 2. (a) Diffusion coefficients of *p*-acetonitrile (closed squares) and *p*-acetone (open circles) as determined by ^{1}H PFG-NMR for different acetone/acetonitrile/ LiTFSI ratios. *d*-acetone and *d*-acetonitrile were used in the formulation of the solutions to assess the dynamics of *p*-acetonitrile and *p*-acetone. The evolution of $D_{acetonitrile}/D_{acetone}$ ratio is shown in the inset. (b) Diffusion coefficients for Li$^+$ (closed triangles) and TFSI$^-$ (open triangles) as determined via ^{7}Li and ^{19}F PFG-NMR. The corresponding D_{Li+}/D_{TFSI-} ratios are shown in the inset. (c) Evolution of the inverse Haven ratios (H^{-1}) for the solutions with different acetone/acetonitrile/LiTFSI ratios.

The values of D at 300K were also determined via MD, as shown in the SI (Fig. S3). Qualitatively, MD's results show a good agreement with PFG-NMR, and quantitatively are comparable with those obtained experimentally at 280K, possibly because of inherent thermodynamic deviations of the simulations[47]. The composition 0:7.3:1, whose ionic concentration is the same as in 3:3:1, was also included in the simulations. In Fig. S3 a comparison between D in these compositions is presented and while no significant difference in D_{Li^+} is observed, D_{TFSI^-} and $D_{acetonitrile}$ are ~20% and ~16% respectively higher with acetone.

The PFG-NMR-determined D_{Li^+} and D_{TFSI^-} were then combined with the experimental conductivities to calculate the so-called inverse Haven ratio (H^{-1}) - the ratio between the experimental conductivities (σ_{exp}) and the ideal ones where no ion-ion correlations occur, that is, the Nernst-Einstein conductivity (σ_{NE}):

$$H^{-1} = \frac{\sigma_{exp}}{\sigma_{NE}};\ \sigma_{NE} = \frac{q^2}{k_B T}(n_+ D_+ + n_- D_-)$$

(1)

where k_B is the Boltzmann constant, q is the elementary charge, D_+ and D_- are the ions' diffusion coefficients, and n_+ and n_- are the corresponding ionic concentrations. H^{-1} inversely depicts the degree of cation-anion correlations and as shown in Fig. 2c, H^{-1} < 1 for all samples at temperatures ≥ 280 K, as expected for concentrated solutions. For comparison, the composition 1:3:1 presents at 280K and 300K values of H^{-1} higher than those reported for an acetonitrile/LiTFSI = 3:1 mixture[46]. That is, at low concentrations and temperatures close to ambient, acetone promotes a better separation between the ions as one could expect upon the addition of a polar co-solvent. Below 280K, however, the influence of the addition of acetone cannot be exaplained as a simple dilution process. H^{-1} is exceptionally high and reaches values above the unity. Here, experimental deviations must be considered, for example, because of the difference in the vapor pressures of acetonitrile and acetone in the experimental container and consequent variations in the concentration of the solution under analysis. Another possibility is the presence of large ion-solvent complexes that may contribute to the experimental conductivity at low temperatures but are too slow to be detected by PFG-NMR. Even considering these hypotheses, the unusual behavior of H^{-1} must be investigated in future works.

In the compositions 3:3:1 and 9:3:1, an unexpected increase in the cation-anion correlations is indicated by the low values of H^{-1}, which are comparable with the one reported for a co-solvent-free acetonitrile/LiTFSI = 3:1 solution[46]. Here, it is clear that the addition of acetone to the acetonitrile/LiTFSI solution does not constitute a simple dilution process, in which a reduction of cation-anion correlations should occur. In principle, one could argue that our observations are in line with a previous report with aqueous LiTFSI solutions, where a slight decrease in ionicity was detected as the ionic concentrations changed from 5 to 1 mol.kg^{-1} [18]. For the aqueous systems, however, the ionicities are much higher in this concentration range and a reduction in conductivity was also detected, which is not the case in the acetone-containing solutions. Therefore, especially in 9:3:1, the formation of ion-ion correlations promoted by acetone and reduction of ionic concentration, do not surpass the benefits of the reduction in viscosity and the enhancement of vehicle-type ionic transport.

To comprehend the effects of acetone on the ion-ion and ion-solvent correlations within the solutions and elucidate the experimental results presented so far, we have used MD to determine the radial distribution functions (RDFs), shown in Fig. 3a, b, and c, and coordination numbers of the cations by acetonitrile, displayed in Fig. 3d. For $TFSI^-$, coordination numbers by the solvents were not accurately determined because of the absence of clear minima in the RDFs. Details of the calculations are given

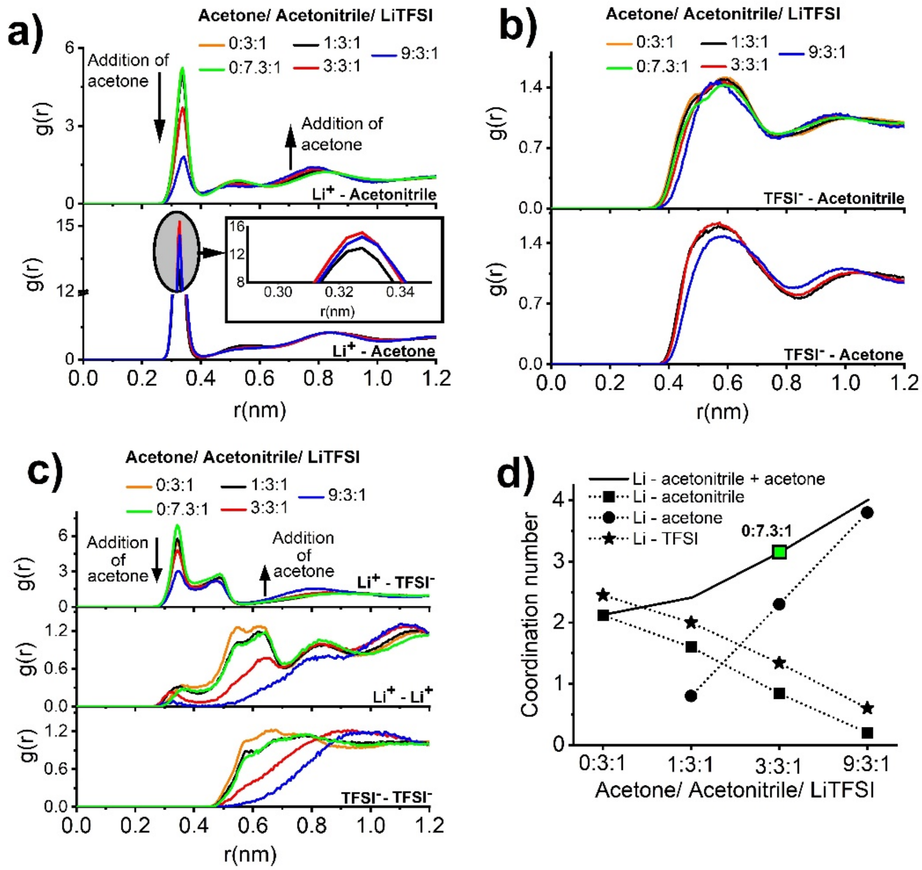

Fig. 3. (a) RDFs depicting the Li$^+$-solvent interactions. In the top panel, the curves from 0:3:1, 0:7.3:1, and 3:3:1 are nearly superposed and the arrows highlight the evolution of different populations of acetonitrile around the cations. (b) RDFs depicting the TFSI$^-$-solvent interactions. In the top panel, the curves from 0:3:1 and 1:3:1 are nearly superposed as well as those from 0:7.3:1 and 3:3:1. In the bottom panel, the curves from 1:3:1 and 3:3:1 are nearly superposed. (c) The RDFs depict the ion-ion interactions. In the top panel, the curves from 0:3:1 and 1:3:1 are nearly superposed, as well as 0:7.3:1 and 1:3:1 in the mid and bottom panels. (d) Evolution of the coordination numbers of Li$^+$ by the solvents and the anions and the green dot indicates the coordination of Li$^+$ by acetonitrile in the composition 0:7.3:1.

in the SI, Section S1a, and one should notice that the RDFs were calculated considering the center of mass of the molecules and, therefore, represent intermolecular interactions. From the results in Fig. 3a and d, acetone gradually replaces acetonitrile in the coordination of Li$^+$ and, most importantly, changes the profile of the Li-acetonitrile interactions. In Fig. 3a, while the peak in the RDF at ~ 0.4 nm due to the interactions between Li$^+$ and acetonitrile's *N*-atoms decreases, the interactions between Li$^+$ and the solvent's *C*-atoms (~ 0.8 nm) subtly increase indicating radial coordination of the cations by acetonitrile[48]. Overall, the Li-solvent interactions in the concentration 0:7.3:1 are more comparable with the compositions 0:3:1 and 1:3:1 than with 3:3:1. As shown in Fig.3b, the effect of the addition of acetone on the anions' solvation is not clear but there is a smooth shift of the acetonitrile molecules to larger distances. For the composition 0:7.3:1, as the green dot in Fig. 3d shows, the number of solvent molecules coordinating Li$^+$ is similar to the composition 3:3:1.

From the composition 0:3:1 to 1:3:1, the Li$^+$-TFSI$^-$ coordination decreases in agreement with the behavior of H^{-1} (considering the H^{-1} reported elsewhere for 0:3:1[46]). Still, the RDFs (Fig.3c) show very similar distributions of TFSI$^-$ around Li$^+$ in these compositions. For the compositions 3:3:1 and 9:3:1, the evolution of H^{-1} exposes subsequent

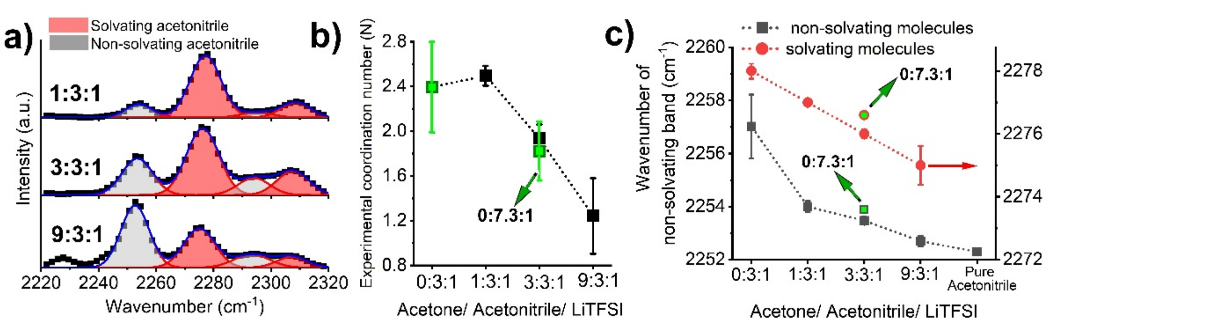

Fig. 4. Results extracted from the analyses of IR experiments with the different acetone/acetonitrile/LiTFSI solutions. (a) Visual presentation of the discrimination between the vibrations from solvating and non-solvating acetonitrile molecules. (b) behavior of N for the different compositions, (c) frequencies of the main vibrations from coordinating and non-coordinating acetonitrile molecules.

increases in the cation-anion interactions with the addition of acetone, but the coordination numbers indicate otherwise. Interestingly, the RDFs in Fig.3c also show a change in the profile of the Li^+-$TFSI^-$ interactions. While acetone damps the interactions between Li^+ and the anion's O-atoms (peak at ~ 0.3 nm) (and these were considered for the calculation of the coordination numbers), the gradual increase in the peak at ~ 0.8 nm indicates interactions between Li^+ and the anions' S-atoms[48]. Therefore, the increase in cation-anion correlations led by acetone is not based on the dominant short-range Li-O_{TFSI} interactions but the partial participation of $TFSI^-$ in an extended solvation shell in which Li-S_{TFSI} interactions gain relevance. Yet, a relevant fraction of the anions do not participate in this process and perform fast diffusive motions, as reflected by the evolution of D_{Li^+}/D_{TFSI^-} (Fig.2b).

The increase in acetone's concentration also promotes drastic changes in the cation-cation and anion-anion interactions. As shown in Fig. 3c, the RDFs of the compositions 3:3:1 and 9:3:1 are strongly shifted to higher distances corroborating with the formation of extended solvation (Fig. 3c). This effect is only detected with acetone and the composition 0:7.3:1 presents RDFs much comparable with the composition 1:3:1, despite the 67% higher ionic concentration in the latter. As previously mentioned, even with the formation of extended solvation, D_{Li^+} is nearly the same in the compositions 3:3:1 and 0:7.3:1 (Fig. S3), exposing enhanced mobility guaranteed by acetone.

With IR, it is possible to distinguish the vibrations from coordinating and non-coordinating acetonitrile molecules in the spectral region between 2220 and 2320 cm^{-1}, where the main contributions are from the stretching vibrations from the solvent's $C\equiv N$ bond, as depicted in Fig.4a (data for neat acetonitrile and the compositions 0:3:1 and 0:7.3:1 are displayed in Fig. S4). To explore this feature, we fitted the different contributions with Gaussian curves and determined experimental coordination numbers (N) of Li^+ by acetonitrile as[10,11,49]:

$$\frac{A_{Acn-coord}}{A_{Acn-coord}+A_{Acn-uncoord}} = N\frac{[Li^+]}{[Acn]} \quad (2)$$

where $A_{Acn-coord}$ and $A_{Acn-uncoord}$ are the integrated areas of the bands from the coordinating and uncoordinated acetonitrile molecules, and $[Li^+]$ and $[Acn]$ are the cation's and acetonitrile's concentrations. The evolution of N is displayed in (Fig. 4b). While the MD-based coordination numbers are calculated based on the number of molecules in the first solvation sheath of the cations, the experimental value N is influenced by acetonitrile molecules that are disturbed by the cations regardless of whether they are in the first or outer solvation sheaths. Hence, N is expected to be somewhat higher than the MD-based coordination numbers. When the composition changes from 0:3:1 to 1:3:1, no considerable difference is detected in N indicating that the acetonitrile molecules shifted from the cations' coordination, as pointed by MD, are prone to be allocated in extended solvation shells rather than readily released as free molecules. With subsequent additions of acetone, N decreases and is nearly the same in the compositions 0:7.3:1 and 3:3:1 in contrast with the discrepancy indicated by MD. This is yet another indication that acetonitrile is not fully released as free molecules upon the addition of the co-solvent.

From the fits of the IR bands, we have obtained the following additional information. As shown in Fig.4c, the vibrational frequency of the main band from the non-coordinating fraction of acetonitrile rapidly evolves to the frequency observed for the pure solvent when either acetone or acetonitrile are added to the original solution. This effect is slightly less pronounced with the dilution with acetonitrile. In other words, acetone promotes a chemical environment for the free molecules of acetonitrile closer to the pure solvent, which agrees with the higher mobility of acetonitrile in the composition 3:3:1 as compared with 0:7.3:1 (Fig. S3). For the solvating molecules of acetonitrile, the addition of acetone leads to a reduction in vibrational frequency, which also occurs with the simple dilution with acetonitrile but in a less pronounced manner. We also used IR to evaluate the vibrational features of acetone and $TFSI^-$ [50] (Fig. S5 and S6). For acetone, the results corroborate the discussions made based on the RDFs, and the presence of free and/or weakly interacting molecules of the co-solvent increases with its concentration, concomitantly with an increase in the presence of strongly coordinated molecules. For $TFSI^-$, the IR results show that the S=O bonds are susceptible to the additions of acetone and dilution with acetonitrile, confirming that the O and S atoms of the anions

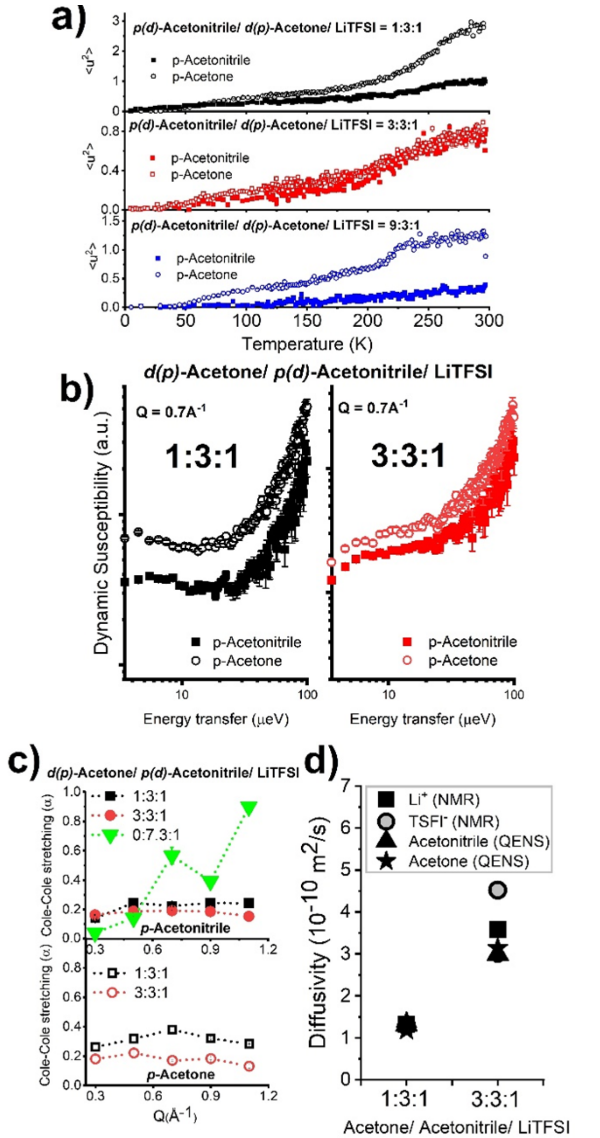

Fig. 5. (a) $<u^2>$ of p-acetonitrile and p-acetone in samples with different compositions. (b) QENS data presented as dynamic susceptibilities at 300K. (c) Cole-Cole stretching parameter. (d) Diffusivities of the solvents obtained via QENS as compared with the ionic conductivities obtained via PFG-NMR.

play key roles in the Li-TFSI coordination. Contrarily, the S-N bonds are not sensitive to the addition of the co-solvent. Lastly, the IR results show that the C-F bonds, which are very much involved in anion-anion interactions[18], seemingly become freer upon the addition of acetone, in agreement with the damping of the $TFSI^-$-$TFSI^-$ interactions suggested by the RDFs in Fig.3c.

Finally, we used quasielastic neutron scattering (QENS) to assess the solutions on a sub-nanometric length scale rather than the micron-scale assessed by PFG-NMR. Therefore, since large and slow solvation complexes co-exist with small and fast ones, the latter are more likely to influence the results from PFG-NMR. In other words, the QENS data can reveal the dynamics of complex solvation structures that may contribute to the conductivity of the electrolytes but are not fully assessed with PFG-NMR. In Fig. 5a, the mean-square displacements, $<u^2>$, obtained at the spectrometer HFBS for the compositions 1:3:1, 3:3:1, and 9:3:1 are presented. The offsets at T > 200K indicate the activation of motions in the samples and p-acetone also presents the activation of methyl rotations around 50K. For the composition 1:3:1, $<u^2>$ at room temperature is higher for p-acetone than p-acetonitrile confirming that the latter is dominant in ionic coordination. In 3:3:1, the displacements from both solvents are almost superposed and in 9:3:1, the larger content of free acetone manifests itself as a higher $<u^2>$.

For the experiments performed at the BASIS spectrometer, the composition 9:3:1 was not prioritized since it presented no advantages in terms of its conductivity (Fig. 1). In Fig. 5b, the QENS data are presented as dynamic susceptibilities at Q = 0.7Å^{-1}, and *p*-acetonitrile and *p*-acetone present similar relaxations in both 1:3:1 and 3:3:1, but the relaxations are faster in the latter. In Fig. S7, the Q-dependence of the dynamic susceptibilities are presented. The dynamic scattering functions of the QENS signals were fitted with a Cole-Cole equation[51] (details in SI) whose stretching factor "α" reflects the diversity of the populations under analysis[52]. As presented in Fig. 5c, "α" is Q-independent for *p*-acetonitrile in the acetone-containing samples and slightly drops from the composition 1:3:1 to 3:3:1. Contrarily, in the composition 0:7.3:1, "α" is strongly Q-dependent and reaches values close to unity indicating that more than a single relaxation is relevant in the signal. For *p*-acetone, "α" is also Q-independent in both the compositions 1:3:1 and 3:3:1. Nevertheless, for *p*-acetone, the somewhat higher values of "α" in the composition 1:3:1 indicate a greater influence of more than a single relaxation in the signal, which contributes to the substantially higher MSD as compared with *p*-acetonitrile.

The broadenings of the QENS signals were fitted with a DQ^2 diffusion law (details in SI, Fig. S8) and the obtained diffusivities are displayed in Fig. 5d ($D_{Li^+}$and D_{TFSI^-} determined with PFG-NMR are reproduced in the figure). For the composition 1:3:1, $D_{\text{acetonitrile}}$ is equivalent to D_{acetone} considering the experimental errors ($D_{\text{acetonitrile}}$ = 1.31 ± 0.08 x 10^{-10} m^2/s and D_{acetone} = 1.18 ± 0.01 x 10^{-10} m^2/s), which are also comparable with $D_{Li^+}$and D_{TFSI^-}. Therefore, this is further confirmation that a considerable fraction of the ions and the solvents coexist as clusters within the solution. In the composition 3:3:1, $D_{\text{acetonitrile}}$ is still very similar to D_{acetone} ($D_{\text{acetonitrile}}$ = 2.99 ± 0.16 x 10^{-10} m^2/s and D_{acetone} = 3.14 ± 0.02 x 10^{-10} m^2/s) but slower than $D_{Li^+}$and D_{TFSI^-}. Therefore, the presence of the solvents in slow-moving structures is dominant in the QENS experiment, but faster motions of the ions independently of these clusters are enabled. In the composition 0:7.3:1, $D_{\text{acetonitrile}}$ = 4.29 ± 0.39 x 10^{-10} m^2/s, which is higher than in the composition 3:3:1, in contradiction with the MD results, likely due to a model-dependent artifact, given the behavior of the stretching parameter.

We have also used QENS to investigate the solutions with the compositions 1:3:1 and 3:3:1 under confinement in mesoporous carbon, as presented in detail in Section S3. Although these are preliminary results, they provide an impression of how the configuration of the bulk solutions may affect their behavior while confined in an electrode-like matrix. Briefly, in the composition 1:3:1, we observe that acetone is more prone to interact with the carbon walls as it is more often found as free molecules in the bulk solution. In the composition 3:3:1, both solvents equally interact with the pore walls. As for the remaining mobile molecules within the pores, $D_{\text{acetonitrile}}$ and D_{acetone} cannot be distinguished beyond the experimental errors in the composition 1:3:1, indicating that both solvents either diffuse together as part of the ion-solvent complexes formed in the bulk solutions or are subjected to similar interactions with the the carbon matrix. In the composition 3:3:1, $D_{\text{acetonitrile}}$ and D_{acetone} are still comparable, but the detectable difference between the diffusivities may indicate a likely change in the original solvation structures formed in the bulk. Overall, $D_{\text{acetonitrile}}$ and D_{acetone} tend to decrease when the composition changes from 1:3:1 to 3:3:1 (although the difference for D_{acetone} is not beyond the errors), which may be related to the formation of larger solvation structures in the bulk as the concentration of acetone increases. Finally, in all cases, the diffusivities are higher than those obtained for the bulk samples as reported for several confined fluids [53,54].

Conclusions

In the present work, we used acetone as a co-solvent in an acetonitrile/LiTFSI concentrated solution and evaluated the effects on structure and dynamics within the system. The co-solvent has concentration-dependent effects that can be tuned to promote different solvation structures and higher conductivities than those obtained with acetone-free solutions with the same ionic concentrations. At low concentrations, acetone slightly shifts acetonitrile to an extended solvation shell but the original solvation structures around the ions are mostly preserved. Then, high-concentration clusters are formed in the solution likewise expected with low polar co-solvents. By increasing acetone's concentration, the profile of the solvation structures gradually changes promoting the formation of Li^+-acetonitrile and Li^+-$TFSI^-$ interactions with different natures than those observed in the original solution. Regarding the Li-acetonitrile coordination, the interactions between the cations and the solvent's *C*-atoms in extended solvation shells are favored at expense of the presence of acetonitrile in the cation's first solation shell. For the cation-anion correlations, these are promoted by acetone thus not following the trend expected for a simple dilution with polar co-solvents. These interactions, however, are not based on the direct coordination between Li^+ and the anions. Instead, the cation-anion correlations occur via long-range interactions in which $TFSI^-$'s *S*-atoms play an important role. Lastly, either at low or high concentrations, acetone leads the non-coordinating acetonitrile molecules (that is those devoid of influence from the ions) to exhibit vibrational features resembling the pure solvent as detected by IR spectrometry, which is possibly an additional facilitating factor for ionic diffusion.

ASSOCIATED CONTENT

Supporting Information

The Supporting Information is available free of charge on the ACS Publications website.

Experimental details and data analysis, additional results from MD, IR, and QENS, and QENS analysis of solutions confined in porous carbon.

AUTHOR INFORMATION

Corresponding Authors

* M. L. Martins. E-mail: longomartiml@ornl.gov.
* R.L. Sacci. E-mail: saccirl@ornl.gov
* E. Mamontov. E-mail: mamontove@ornl.gov.

Author Contributions

MLM performed the QENS experiments at BASIS and data analysis together with EM, prepared the samples, performed IR experiments and data analysis, analyzed the data from molecular dynamics simulations, conductivity experiments, and PFG-NMR, and wrote the paper with input from all authors. RLS performed IR experiments and provided support for sample preparation. IP performed the conductivity measurements with support from APS. XL and RM performed the molecular dynamics calculations with support from PTC. TK and JC performed the PFG NMR experiments with support from MP. MT performed the QENS experiments at HFBS. WG and SD synthesized the mesoporous carbon.

Notes

The authors declare no competing financial interests.

ACKNOWLEDGMENT

This research used resources at the Spallation Neutron Source, a DOE Office of Science User Facility operated by the Oak Ridge National Laboratory. This work was supported as part of the Fluid Interface Reactions, Structures and Transport (FIRST) Center, an Energy Frontier Research Center funded by the U.S. Department of Energy, Office of Science, Office of Basic Energy Sciences. This research used resources of the National Energy Research Scientific Computing Center, a DOE Office of Science User Facility supported by the Office of Science of the U.S. Department of

Energy under Contract No. DE-AC0205CH11231. Oak Ridge National Laboratory is managed by UT-Battelle, LLC, for U.S. DOE under Contract No. DEAC05-00OR22725. The authors are also thankful to Dr. Luke Daemen for providing chemical reagents for the neutron scattering experiments. Access to the HFBS beamlines was provided by the Center for High Resolution Neutron Scattering, a partnership between the National Institute of Standards and Technology and the National Science Foundation under Grant Agreement No. DMR-1508249. Certain commercial material suppliers are identified in this article to foster understanding. Such identification does not imply recommendation or endorsement by the National Institute of Standards and Technology, nor does it imply that the materials or equipment identified are necessarily the best available for the purpose.

REFERENCES

(1) Zubi, G.; Dufo-López, R.; Carvalho, M.; Pasaoglu, G. The Lithium-Ion Battery: State of the Art and Future Perspectives. *Renew. Sustain. Energy Rev.* **2018**, *89*, 292–308.

(2) Scrosati, B.; Hassoun, J.; Sun, Y.-K. Lithium-Ion Batteries. A Look into the Future. *Energy Environ. Sci.* **2011**, *4*, 3287. https://doi.org/10.1039/c1ee01388b.

(3) Blomgren, G. E. The Development and Future of Lithium Ion Batteries. *J. Electrochem. Soc.* **2017**, *164*, A5019–A5025.

(4) Yamada, Y.; Wang, J.; Ko, S.; Watanabe, E.; Yamada, A. Advances and Issues in Developing Salt-Concentrated Battery Electrolytes. *Nat. Energy* **2019**, *4*, 269–280.

(5) Wang, Y.; Yi, J.; Xia, Y. Recent Progress in Aqueous Lithium-Ion Batteries. *Adv. Energy Mater.* **2012**, *2*, 830–840.

(6) Watanabe, M.; Thomas, M. L.; Zhang, S.; Ueno, K.; Yasuda, T.; Dokko, K. Application of Ionic Liquids to Energy Storage and Conversion Materials and Devices. *Chem. Rev.* **2017**, *117*, 7190–7239.

(7) Suo, L.; Hu, Y.-S.; Li, H.; Armand, M.; Chen, L. A New Class of Solvent-in-Salt Electrolyte for High-Energy Rechargeable Metallic Lithium Batteries. *Nat. Commun.* **2013**, *4*, 1481.

(8) Nilsson, V.; Younesi, R.; Brandell, D.; Edström, K.; Johansson, P. Critical Evaluation of the Stability of Highly Concentrated LiTFSI - Acetonitrile Electrolytes vs. Graphite, Lithium Metal and LiFePO4 Electrodes. *J. Power Sources* **2018**, *384*, 334–341. https://doi.org/10.1016/J.JPOWSOUR.2018.03.019.

(9) Lundgren, H.; Scheers, J.; Behm, M.; Lindbergh, G. Characterization of the Mass-Transport Phenomena in a Superconcentrated LiTFSI:Acetonitrile Electrolyte. *J. Electrochem. Soc.* **2015**, *162*, A1334–A1340. https://doi.org/10.1149/2.0961507jes.

(10) Yamada, Y.; Furukawa, K.; Sodeyama, K.; Kikuchi, K.; Yaegashi, M.; Tateyama, Y.; Yamada, A. Unusual Stability of Acetonitrile-Based Superconcentrated Electrolytes for Fast-Charging Lithium-Ion Batteries. *J. Am. Chem. Soc.* **2014**, *136*, 5039–5046.

(11) Seo, D. M.; Borodin, O.; Han, S.-D.; Boyle, P. D.; Henderson, W. A. Electrolyte Solvation and Ionic Association II. Acetonitrile-Lithium Salt Mixtures: Highly Dissociated Salts. *J. Electrochem. Soc.* **2012**, *159*, A1489.

(12) Suo, L.; Borodin, O.; Gao, T.; Olguin, M.; Ho, J.; Fan, X.; Luo, C.; Wang, C.; Xu, K. "Water-in-Salt" Electrolyte Enables High-Voltage Aqueous Lithium-Ion Chemistries. *Science (80-.).* **2015**, *350*, 938–943. https://doi.org/10.1126/science.aab1595.

(13) Nilsson, V.; Kotronia, A.; Lacey, M.; Edström, K.; Johansson, P. Highly Concentrated LiTFSI–EC Electrolytes for Lithium Metal Batteries. *ACS Appl. Energy Mater.* **2020**, *3*, 200–207. https://doi.org/10.1021/acsaem.9b01203.

(14) Nilsson, V.; Bernin, D.; Brandell, D.; Edström, K.; Johansson, P. Interactions and Transport in Highly Concentrated LiTFSI-based Electrolytes. *ChemPhysChem* **2020**, *21*, 1166–1176. https://doi.org/10.1002/cphc.202000153.

(15) Okoshi, M.; Chou, C.-P.; Nakai, H. Theoretical Analysis of Carrier Ion Diffusion in Superconcentrated Electrolyte Solutions for Sodium-Ion Batteries. *J. Phys. Chem. B* **2018**, *122*, 2021. https://doi.org/10.1021/acs.jpcb.7b10589.

(16) Lim, J.; Park, K.; Lee, H.; Kim, J.; Kwak, K.; Cho, M. Nanometric Water Channels in Water-in-Salt Lithium Ion Battery Electrolyte. *J. Am. Chem. Soc.* **2018**, *140*, 15661–15667. https://doi.org/10.1021/jacs.8b07696.

(17) Andersson, R.; Årén, F.; Franco, A. A.; Johansson, P. Ion Transport Mechanisms via Time-Dependent Local Structure and Dynamics in Highly Concentrated Electrolytes. *J. Electrochem. Soc.* **2020**, *167*, 140537. https://doi.org/10.1149/1945-7111/abc657.

(18) Borodin, O.; Suo, L.; Gobet, M.; Ren, X.; Wang, F.; Faraone, A.; Peng, J.; Olguin, M.; Schroeder, M.; Ding, M. S.; et al. Liquid Structure with Nano-Heterogeneity Promotes Cationic Transport in Concentrated Electrolytes. *ACS Nano* **2017**, *11*, 10462–10471.

(19) Azov, V. A.; Egorova, K. S.; Seitkalieva, M. M.; Kashin, A. S.; Ananikov, V. P. "Solvent-in-Salt" Systems for Design of New Materials in Chemistry, Biology and Energy Research. *Chem. Soc. Rev.* **2018**, *47*, 1250–1284. https://doi.org/10.1039/C7CS00547D.

(20) Martins, M. L.; Sacci, R. L.; Sanders, N. C.; Tyler, J. L.; Matsumoto, R.; Popov, I.; Guo, W.; Dai, S.; Cummings, P. T.; Sokolov, A. P.; et al. Addition of Chloroform in a Solvent-in-Salt Electrolyte: Outcomes in the Microscopic Dynamics in Bulk and Confinement. *J. Phys. Chem. C* **2020**, *124*, 22366–22375.

(21) Moon, H.; Mandai, T.; Tatara, R.; Ueno, K.; Yamazaki, A.; Yoshida, K.; Seki, S.; Dokko, K.; Watanabe, M. Solvent Activity in Electrolyte Solutions Controls Electrochemical Reactions in Li-Ion and Li-Sulfur Batteries. *J. Phys. Chem. C* **2015**, *119*, 3957–3970. https://doi.org/10.1021/jp5128578.

(22) Cataldo, F. A Revision of the Gutmann Donor Numbers of a Series of Phosphoramides Including TEPA. *Eur. Chem. Bull.* **2015**, *4*, 92–97.

(23) Cui, J.; Kobayashi, T.; Sacci, R. L.; Matsumoto, R. A.; Cummings, P. T.; Pruski, M. Diffusivity and Structure of Room Temperature Ionic Liquid in Various Organic Solvents. *J. Phys. Chem. B* **2020**, *124*, 9931–9937.

(24) mBuild GitHub Landing Page https://github.com/mosdef-hub/mbuild (accessed Mar 16, 2020).

(25) Klein, C.; Sallai, J.; Jones, T. J.; Iacovella, C. R.; McCabe, C.; Cummings, P. T. A Hierarchical, Component Based Approach to Screening Properties of Soft Matter; Snurr, R. Q., Adjiman, C. S., Kofke, D. A., Eds.; Springer Singapore: Singapore, 2016; pp 79–92. https://doi.org/10.1007/978-981-10-1128-3_5.

(26) Martínez, L.; Andrade, R.; Birgin, E. G.; Martínez, J. M. PACKMOL: A Package for Building Initial Configurations for Molecular Dynamics Simulations. *J. Comput. Chem.* **2009**, *30*, 2157–2164.

(27) Klein, C.; Summers, A. Z.; Thompson, M. W.; Gilmer, J. B.; McCabe, C.; Cummings, P. T.; Sallai, J.; Iacovella, C. R. Formalizing Atom-Typing and the Dissemination of Force Fields with Foyer. *Comput. Mater. Sci.* **2019**, *167*, 215–227.

(28) Wang, J.; Wolf, R. M.; Caldwell, J. W.; Kollman, P. A.; Case, D. A. Development and Testing of a General Amber Force Field. *J. Comput. Chem.* **2004**, *25*, 1157–1174. https://doi.org/10.1002/jcc.20035.

(29) MoSDeF GitHub Landing Page https://github.com/mosdefhub (accessed Mar 16, 2020).

(30) Summers, A. Z.; Gilmer, J. B.; Iacovella, C. R.; Cummings, P. T.; MCabe, C. MoSDeF, a Python Framework Enabling Large-Scale Computational Screening of Soft Matter: Application to Chemistry-Property Relationships in Lubricating Monolayer Films. *J. Chem. Theory Comput.* **2020**, *16*, 1779–1793. https://doi.org/10.1021/acs.jctc.9b01183.

(31) Adorf, C. S.; Dodd, P. M.; Ramasubramani, V.; Glotzer, S. C. Simple Data and Workflow Management with the Signac Framework. *Comput. Mater. Sci.* **2018**, *146*, 220–229.

(32) Adorf, C. S.; Ramasubramani, V.; Dice, B. D.; Henry, M. M. .; Dodd, P. M.; Glotzer, S. C. Glotzerlab/Signac (Version 1.0.0). Zenodo. 2019.

(33) Ramasubramani, V.; Adorf, C. S.; Dodd, P. M.; Dice, B. D.; Glotzer, S. C. Signac: A Python Framework for Data and Workflow Management. In *Proceedings of the 17th Python in Science Conference*; Akici, F., Lippa, D., Niederhut, D., Pacer, M., Eds.; 2018; pp 152–159. https://doi.org/10.25080/Majora-4af1f417-016.

(34) Vanquelef, E.; Simon, S.; Marquant, G.; Garcia, E.; Klimerak, G.; Delepine, J. C.; Cieplak, P.; Dupradeau, F.-Y. R.E.D. Server: A Web Service for Deriving RESP and ESP Charges and Building Force Field Libraries for New Molecules and Molecular Fragments. *Nucleic Acids Res.* **2011**, *39*, W511–W517.

(35) Canongia Lopes, J. N.; Pádua, A. A. H. CL&P: A Generic and Systematic Force Field for Ionic Liquids Modeling. *Theor. Chem. Acc.* **2012**, *131*, 1129. https://doi.org/10.1007/s00214-012-1129-7.

(36) Canongia Lopes, J. N.; Deschamps, J.; Pádua, A. A. H. Modeling Ionic Liquids Using a Systematic All-Atom Force Field. *J. Phys. Chem. B* **2004**, *108*, 2038–2047. https://doi.org/10.1021/jp0362133.

(37) Thompson, M. W.; Matsumoto, R.; Sacci, R. L.; Sanders, N. C.; Cummings, P. T. Scalable Screening of Soft Matter: A Case Study of Mixtures of Ionic Liquids and Organic Solvents. *J. Phys. Chem. B* **2019**, *123*, 1340–1347. https://doi.org/10.1021/acs.jpcb.8b11527.

(38) Abraham, M. J.; Murtola, T.; Schulz, R.; Páll, S.; Smith, J. C.; Hess, B.; Lindahl, E. GROMACS: High Performance Molecular Simulations through Multi-Level Parallelism from Laptops to Supercomputers. *SoftwareX* **2015**, *1–2*, 19–25. https://doi.org/10.1016/j.softx.2015.06.001.

(39) McGibbon, R. T.; Beauchamp, K. A.; Harrigan, M. P.; Klein, C.; Swails, J. M.; Hernández, C. X.; Schwantes, C. R.; Wang, L.-P.; Lane, T. J.; Pande, V. S. MDTraj: A Modern Open Library for the Analysis of Molecular Dynamics Trajectories. *Biophys. J.* **2015**, *109*, 1528–1532.

(40) Yang, Y.; Takahashi, M.; Kawazoe, Y. Atomic Ordering Recognized by Convergence Characteristics of the Radial Distribution Function. *Solid State Commun.* **2008**, *146*, 468–471. https://doi.org/10.1016/j.ssc.2008.04.004.

(41) Martins, M. L.; Gates, W. P.; Michot, L.; Ferrage, E.; Marry, V.; Bordallo, H. N. Applied Clay Science Neutron Scattering , a Powerful Tool to Study Clay Minerals. *Appl. Clay Sci.* **2014**, *96*, 22–35. https://doi.org/10.1016/j.clay.2014.05.004.

(42) Meyer, A.; Dimeo, R. M.; Gehring, P. M.; Neumann, D. A. The High-Flux Backscattering Spectrometer at the NIST Center for Neutron Research. *Rev. Sci. Instrum.* **2003**, *74*, 2759–2777. https://doi.org/10.1063/1.1568557.

(43) Martins, M. L.; Eckert, J.; Jacobsen, H.; dos Santos, É. C.; Ignazzi, R.; de Araujo, D. R.; Bellissent-Funel, M. C.; Natali, F.; Koza, M. M.; Matic, A.; et al. Probing the Dynamics of Complexed Local Anesthetics via Neutron Scattering Spectroscopy and DFT Calculations. *Int. J. Pharm.* **2017**, *524*, 397–406. https://doi.org/10.1016/j.ijpharm.2017.03.051.

(44) Mamontov, E.; Herwig, K. W. A Time-of-Flight Backscattering Spectrometer at the Spallation Neutron Source, BASIS. *Rev. Sci. Instrum.* **2011**, *82*, 085109.

(45) Mamontov, E.; Smith, R. W.; Billings, J. J.; Ramirez-Cuesta, A. J. Simple Analytical Model for Fitting QENS Data from Liquids. *Phys. B Condens. Matter* **2019**, *566*, 50–54.

(46) Popov, I.; Sacci, R. L.; Sanders, N. C.; Matsumoto, R. A.; Thompson, M. W.; Osti, N. C.; Kobayashi, T.; Tyagi, M.; Mamontov, E.; Pruski, M.; et al. Critical Role of Anion–Solvent Interactions for Dynamics of Solvent-in-Salt Solutions. *J. Phys. Chem. C* **2020**, *124*, 8457–8466.

(47) Sprenger, K. G.; Jaeger, V. W.; Pfaendtner, J. The General AMBER Force Field (GAFF) Can Accurately Predict Thermodynamic and Transport Properties of Many Ionic Liquids. *J. Phys. Chem. B* **2015**, *119*, 5882–5895.

(48) Sodeyama, K.; Yamada, Y.; Aikawa, K.; Yamada, A.; Tateyama, Y. Sacrificial Anion Reduction Mechanism for Electrochemical Stability Improvement in Highly Concentrated Li-Salt Electrolyte. *J. Phys. Chem. C* **2014**, *118*, 14091–14097. https://doi.org/10.1021/jp501178n.

(49) Barthel, J.; Buchner, R.; Wismeth, E. FTIR Spectroscopy of Ion Solvation of LiClO4 and LiSCN in Acetonitrile, Benzonitrile, and Propylene Carbonate. *J. Solution Chem.* **2000**, *29*, 937–954.

(50) Wang, L.; Uosaki, K.; Noguchi, H. Effect of Electrolyte Concentration on the Solvation Structure of Gold/LITFSI-DMSO Solution Interface. *J. Phys. Chem. C* **2020**, *124*, 12381–12389.

(51) Mamontov, E.; O'Neill, H. Microscopic Relaxations in a Protein Sustained down to 160 K in a Non-Glass Forming Organic Solvent. *Biochim. Biophys. Acta - Gen. Subj.* **2017**, *1861*, 3513–3519. https://doi.org/10.1016/j.bbagen.2016.04.024.

(52) Bridges, C. A.; Martins, M. L.; Jafta, C. J.; Sun, X. G.; Paranthaman, M. P.; Liu, J.; Dai, S.; Mamontov, E. Dynamics of Emim+ in [Emim][TFSI]/LiTFSI Solutions as Bulk and under Confinement in a Quasi-Liquid Solid Electrolyte. *J. Phys. Chem. B* **2021**, *125*, 5443–5450. https://doi.org/10.1021/acs.jpcb.1c02383.

(53) Berrod, Q.; Ferdeghini, F.; Judeinstein, P.; Genevaz, N.; Ramos, R.; Fournier, A.; Dijon, J.; Ollivier, J.; Rols, S.; Yu, D.; et al. Enhanced Ionic Liquid Mobility Induced by Confinement in 1D CNT Membranes. *Nanoscale* **2016**, *8*, 7845–7848.

(54) Filippov, A.; Gnezdilov, O. I.; Hjalmarsson, N.; Antzutkin, O. N.; Glavatskih, S.; Furó, I.; Rutland, M. W. Acceleration of Diffusion in Ethylammonium Nitrate Ionic Liquid Confined between Parallel Glass Plates. *Phys. Chem. Chem. Phys.* **2017**, *19*, 25853–25858.

TOC Graphic